Proc. of the XI Int. Conf. — Ion Implantation and other Applications of Ions and Electrons, Kazimierz Dolny 2016

Modeling, Simulation and Characterization of Aluminum Implantation in 4H-SiC for Large-Area Photodiode Technology

A. Kociubiński*
Lublin University of Technology, Nadbystrzycka 38a, 20-618 Lublin, Poland

Simulation, modeling and characterization of the aluminum ion implantation in 4H-SiC for large-area photodiode technology have been presented in this paper. Modeling and simulation have been performed using the SRIM and TCAD software EDA environments. Main goals were to present and compare the single vs. multiple ion implantation results as well to develop processes leading to achieve required implantation profiles.

DOI: 10.12693/APhysPolA.132.225
PACS/topics: 85.30.De, 85.30.Kk

1. Introduction

Silicon carbide is of considerable interest for the development of optoelectronic and high-temperature devices and is currently perhaps the most promising material for these applications. SiC photodiodes robustness is well known for ultraviolet light detection even in the harsh environment due to high quantum efficiency in a wide UV range, excellent for visible, and blind for the infrared spectral range (excluding UV filters), low dark current and high speed. The 4H (hexagonal) polytype of silicon carbide is the most commonly used for device manufacturing. 4H-SiC has a three times wider band gap, a thermal conductivity 2–3 times higher and a dielectric strength 10 times higher than silicon. This means that the SiC devices can be made smaller, lose less energy, switch faster, work at higher temperatures, and that expensive cooling peripherals become redundant. However, the silicon based process steps are not fully-compatible for the SiC device technology. Especially, doping by diffusion is not possible in SiC. The high diffusion temperatures (around even 2000 °C) make diffusion profiles hardly controllable and difficult to perform, and any application of masking techniques, e.g. used in silicon technology, has not been possible so far [1–3].

A promising way to dope the defined regions of SiC seems to be ion implantation in combination with appropriate annealing processes. Due to serious problems related to the annealing of damaged surface after the ion bombardment most of doping implantations have been carried out at target elevated temperature. The most popular acceptor impurities in SiC are aluminum and boron. For making low-resistance ohmic contacts on the devices intended for room temperature operation, the Al implantation is preferred due to its lower carrier ionization energy compared to B ($\approx$ 200 meV for Al vs. $\approx$ 285 meV for B in 4H polytype) [4]. The ion implantation process for SiC causes crystal damage. High implantation fluences result in formation of an amorphous SiC surface layer [5]. In order to recover the crystal damage and activate the dopants, a high temperature annealing step over 1500 °C is required. Stability of post-implantation dopant annealing reduces the implantation-induced damages and makes aluminum the preferred element to form p-type regions in SiC [6, 7].

The SiC photodiode structures are usually formed by the implantation process with multiple ion energies and fluences performed from the aluminum ion sources. A key importance aspect of aluminum implantation in 4H-SiC is a one of the steps in photodiode technologies. A set of modelling and simulation techniques as well as the results concerning implantation into 4H-SiC and electrical characteristics have been presented. To achieve a required implantation profile in the SiC substrate it is needed to perform not a single, but series combination of single — called — implantation processes with different energies and fluences. Due to the above mentioned reasons as well as material and operation costs, software verification is very important as one of the steps in SiC and the other devices development and product engineering.

Simulation and modelling works presented in this paper have been performed using the SRIM and TCAD environments. Single implantation results are presented and compared with effects of the implantation with multiple ion energies and fluences. As discussed below, ion implantation process with multiple energies and fluences leads to achieve required profiles correlated with the results of electrical simulations of $p{-}i{-}n$ junction.

2. Modelling of aluminum implantation

Silicon carbide wafers are more expensive in comparison to silicon ones. Therefore the computer assisted analysis of simulation results based on modelling is so important to reduce time and costs of technology development [8–10].

*corresponding author; e-mail: akociub@semiconductor.pl

Typical ion implantation processes are performed at room temperature, but high fluences of implanted ions (above 10^{16} cm^{-2}) result in high radiation damage hard to recover even under high temperature post-implantation annealing process (PIA). Higher temperature of implantation process varied within the range of 400 °C to 800 °C and high temperature PIA within the range of 1500–1800 °C reveal the way to resolve the above mentioned constraints and decrease degree of surface radiation damage. Most of the industrial and research implanters are not geared for implantations in this temperature range [11–14].

Therefore Al on implantation in SiC was also preceded by very detailed computer modelling and simulation by the well-known SRIM-2013 [15] and Silvaco TCAD EDA environment. Main goals of performed simulations were values of ion fluence and energy to obtain a required implantation profile, also as results of multiple ion implantation [4, 16].

Main boundary conditions were the maximally flat (quasi flat, box-shape) implantation profiles. According to the theoretical knowledge, experimental measurement data and first simulation results it was assumed and confirmed that the minimum implantation energy should be around 55 keV and not exceed 250 keV. Such implantation processes with the above mentioned parameters prove to be reliable and possible to perform in the ion implanter — UNIMAS [17]. Series of dedicated simulations were performed for single and multiple implantation processes. To achieve a flat distribution of p-type dopant and a box-shaped profile, the multiple energy Al^+ ion implantation process was applied according to Table I. The total fluence was 7×10^{14} cm^{-2}.

To obtain the required implantation parameters (fluence, quasi-flat profile) it is necessary to perform the 4-stage multiple implantation process in the order from the maximum to the minimum implantation energy (Fig. 1). The dopant profiles with the post-implantation annealing calculated by Silvaco TCAD are shown in Fig. 2. The circular 4 mm photodiodes were fabricated by the multiple ion implantation process using the 4H-SiC substrate.

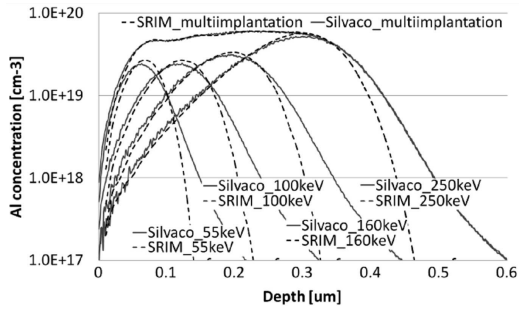

Fig. 1. Comparison of the simulation results of SRIM and Silvaco TCAD programs for the aluminum single implantations with different energies (55–250 keV). The chart also shows the sum of single simulations as a result of complete multiple implantation.

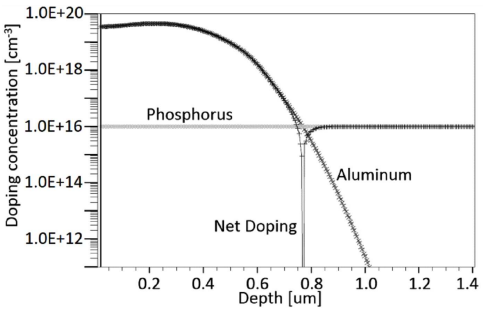

Fig. 2. Silvaco TCAD model of full implantation profile after the annealing process. The complete junction depth at 0.78 μm is observed.

TABLE I

Al^+ ion implantation energies and fluences for the optimized implantation process.

Implantation energies [keV]	Al fluence [cm^{-2}]
250	3.7×10^{14}
160	1.7×10^{14}
100	1.0×10^{14}
55	6.5×10^{13}

3. Photodiode fabrication and characterization

Experimental investigations were carried out on the commercially available 4H-SiC wafers purchased from Cree Research Inc. The average micropipe density was below 7.97 cm^{-2}. The epitaxial structure is composed of two layers and it was grown on the n^+-type, 3 inch diameter substrate with 0.021 Ω cm resistivity, 4° off-axis. First, the field-stop of 0.5 μm thick layer was deposited with the n-type doping of 10^{18} cm^{-3}. The second epilayer is 4.5 μm thick with the n-type doping of 1.52×10^{16} cm^{-3} (Fig. 3).

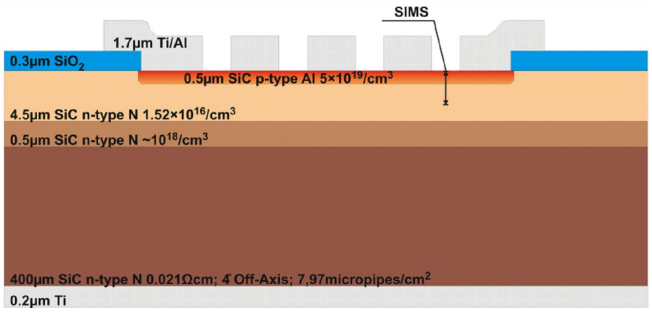

Fig. 3. Schematic cross-section of modelled SiC photodiode.

The SiC wafers used for testing ion implantation processes were cleaned using the RCA procedure in order to remove organic and natural oxides. During the ion

implantation process the SiC substrate was heated up to 500 °C. Implantation energies and fluences of Al^+ ions were selected based on SRIM 2013 simulation and modelling results.

One of the problems in ion implantation technology is activation of the p-type dopants if the acceptor concentration exceeds the solubility limit in SiC. Higher annealing temperatures and longer annealing times are required to produce device–quality p-type layers. The $p{-}i{-}n$ device formed by the above mentioned specification of fabrication process was annealed in the high temperature post implantation annealing process for the purpose of SiC recrystallization and Al^+ ions activation. Annealing of implanted SiC needs to be performed in high-purity inert ambient gas like argon. High temperature annealing in ambient nitrogen produces nitride layers on the surface of SiC. The annealing processes were performed during 20 min process using epitaxy dedicated reactor under the pressure of 100 hPa at the temperature of 1600 °C in ambient argon. The electrodes in the n-type and p-type regions were formed by Ti/Al and Ti magnetron sputtering (lift-off technique). Both contacts were annealed simultaneously at 1050 °C for 5 min in argon. The junction is passivated with a SiO_2 layer. Dopant depth profiles were obtained using secondary ion mass spectroscopy — SIMS (Fig. 4). Previously a similar technology with small devices with epitaxial [18] and implanted [19, 20] junction was applied. The small implantation junctions of 4H-SiC were used to build a dual-band photodetector [21, 22].

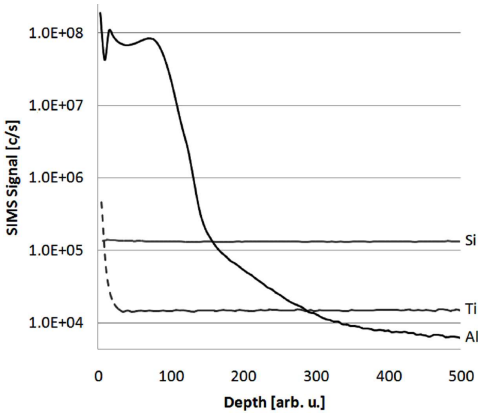

Fig. 4. SIMS depth profiles of Al^+-implanted 4H-SiC at 500 °C after post-annealing at 1600 °C.

For sensing applications the term "large area" is defined to be larger than 1 mm^2 [23]. The device under investigation has a circle geometry with a diameter of 4.0 mm and it was located in the center of 1 cm^2 chip. The top contact electrode was designed as a fishnet pattern with open hexagon windows. The window width was 400 μm and the current collection electrode width was 54 μm. The structure of the SiC-based $p{-}i{-}n$ device was mounted on the 1 inch diameter printed boards as shown in Fig. 5, allowing them to be incorporated into the SM1 standard holders with the optoelectronic equipment. The selected technology and electrode topography are adequate for their intended use in the optoelectronic devices under development for intelligent classification of organic and biological fluids [24–27].

Fig. 5. SiC photodiode structure mounted on the 1 inch diameter printed board.

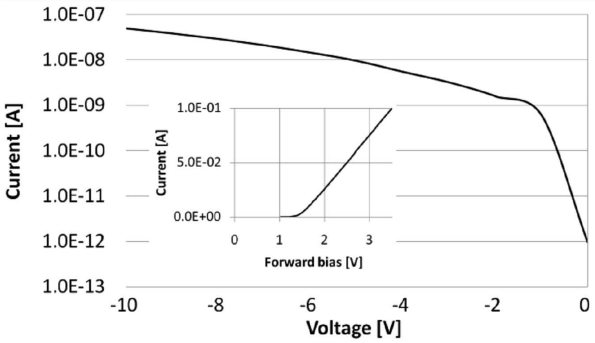

Fig. 6. Reverse $I{-}V$ characteristics of the $p{-}n$ junction diode at room temperature in a shielded fixture. The left bottom part shows $I{-}V$ characteristics.

In order to investigate the diode quality, the electrical properties of the SiC-based $p{-}i{-}n$ device were studied at room temperature. $I{-}V$ characteristics were measured using KEITHLEY SMU 236. The dark current of this device was below 0.6 nA level at the reverse bias of 1 V. As shown in Fig. 6, the dark current increased from 0.6 nA to 50 nA when the applied reverse bias increased from 1 to 10 V. For a circular diode of 4 mm diameter, the dark current density was 395 nA/cm^2 at –5 V.

Capacitance measurements were performed using the precision Keysight B1500A analyzer. The reciprocal of the squared capacitance ($1/C^2$) for the reverse bias in the range of 0–10 V is shown in Fig. 7. The linearity of $1/C^2{-}V$ curve shows good uniformity of doping concentration within the active layer.

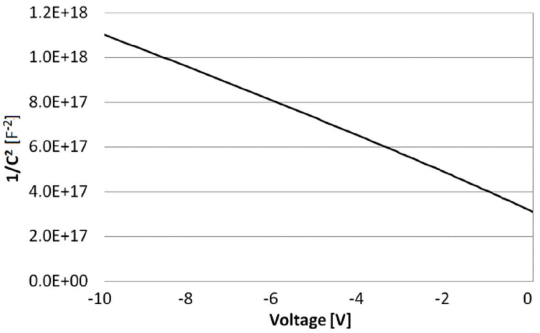

Fig. 7. Reciprocal of the squared capacitance ($1/C^2$) for the reverse bias in the range of 0–10 V.

4. Conclusions

Simulation results of Al implantation process using two different software tools are presented in this paper. SRIM is a typical simulator only for ion implantation, TCAD is a full technology simulator and its important advantage is the possibility of simulating other even full technological processes e.g. combined processes like diffusion with annealing after implantation (post-implantation annealing). The device has good rectifying $I-V$ characteristics and the experimental reverse current density was found to be about 395 nA/cm^2 at –5 V at room temperature. All these results obtained using a large area detector compared to the similar $p-n$ junction devices proposed in the literature make it the state of art among the UV light solid-state detectors currently available.

Acknowledgments

This paper has been partially supported by the NCBiR/PGNiG grant "Polish Technology for Shale Gas", task T3.1 "Multiparametric sensor of liquid surface monitoring as possible methane source".

With extend gratitude to Prof. Jerzy Żuk, Dr. Michał-Borecki and Dr. Mariusz Sochacki, without whose support this article would not have been written and would not have acquired its present form.

References

[1] S.E. Saddow, A. Agarwal, *Advances in Silicon Carbide Processing and Applications*, Artech House, 2004.

[2] B.J. Baliga, *Silicon Carbide Power Devices*, World Sci, 2005.

[3] T. Kimoto, J.A. Cooper, *Fundamentals of Silicon Carbide Technology: Growth, Characterization, Devices and Applications*, Wiley, 2014.

[4] M.V. Rao, *Solid State Electron.* **47**, 213 (2003).

[5] E. Wendler, A. Heft, W. Wesch, *Nucl. Instrum. Methods Phys. Res. B* **141**, 105 (1998).

[6] M. Rambach, F. Schmid, M. Krieger, L. Frey, A.J. Bauer, G. Pensl, H. Ryssel, *Nucl. Instrum. Methods Phys. Res. B* **237**, 68 (2005).

[7] V.A. Gubanov, C.Y. Fong, *Appl. Phys. Lett.* **75**, 88 (1999).

[8] T. Bieniek, G. Janczyk, P. Janusz, J. Szynka, P. Grabiec, A. Kociubiński, M. Ekwińska, D. Tomaszewski, A. Malinowski, *J. Telecommun. Inf. Technol.* **1**, 34 (2010).

[9] D. Ortloff, T. Schmidt, K. Hahn, T. Bieniek, G. Janczyk, R. Brück, *MEMS Product Engineering*, Springer, Vienna 2014.

[10] A. Kociubiński, T. Bieniek, G. Janczyk, *Acta Phys. Pol. A* **125**, 1374 (2014)).

[11] J. Romanek, D. Grambole, F. Herrmann, M. Voelskow, M. Posselt, W. Skorupa, J. Żuk, *Nucl. Instrum. Methods Phys. Res. B* **251**, 148 (2006).

[12] A. Heft, E. Wendler, T. Bachmann, E. Glaser, W. Wesch, *Mater. Sci. Eng. B* **29**, 142 (1995).

[13] F. Pezzimenti, F.G. Della Corte, R. Nipoti, *Microelectron. J.* **39**, 1594 (2008).

[14] M. Rambach, A.J. Bauer, H. Ryssel, *Phys. Status Solidi* **245**, 1315 (2008).

[15] J.F. Ziegler, M.D. Ziegler, J.P. Biersack, *Nucl. Instrum. Methods Phys. Res. B* **268**, 1818 (2010).

[16] F.G. Della Corte, F. Pezzimenti, R. Nipoti, *Microelectron. J.* **38**, 1273(2007).

[17] M. Turek, S. Prucnal, A. Drozdziel, K. Pyszniak, *Nucl. Instrum. Methods Phys. Res. B* **269**, 700 (2011).

[18] A. Kociubiński, M. Duk, D. Teklinska, N. Kwietniewski, M. Sochacki, M. Borecki, *Proc. SPIE* **9228**, 922804 (2014).

[19] A. Kociubiński, M. Duk, M. Masłyk, N. Kwietniewski, M. Sochacki, M. Borecki, M. Korwin-Pawłowski, *Proc. SPIE* **8903**, 89030V (2013).

[20] A. Kociubiński, M. Duk, M. Korona, K. Muzyka, *Proc. SPIE* **9662**, 96620V (2015).

[21] A. Kociubiński, M. Borecki, M. Duk, M. Sochacki, M.L. Korwin-Pawlowski, *Microelectron. Eng.* **154**, 48 (2016).

[22] A. Kociubinski, M. Duk, T. Bieniek, G. Janczyk, M. Borecki, in: *Int. 3D Systems Integration Conf. (3DIC), Kinsdale, (Ireland)*, 2014, 15291809.

[23] M. Borecki, A. Kociubiński, M. Duk, N. Kwietniewski, M.L. Korwin-Pawlowski, P. Doroz, J. Szmidt, *Proc. SPIE* **8903**, 89030H (2013).

[24] P. Prus, M. Borecki, M.L. Korwin-Pawlowski, A. Kociubiński, M. Duk, *Proc. SPIE* **9290**, 929009 (2014).

[25] M. Borecki, M.L. Korwin-Pawlowski, M. Duk, A. Kociubiński, J. Frydrych, P. Prus, J. Szmidt,, *Sensors Transduct.* **193**, 11 (2015).

[26] M. Borecki, P. Doroz, P. Prus, P. Pszczolkowski, J. Szmidt, M.L. Korwin-Pawlowski, J. Frydrych, A. Kociubinski, M. Duk, *Int. J. Adv. Syst. Meas.* **7**, 57 (2014).

[27] M. Borecki, P. Doroz, J. Szmidt, M.L. Korwin-Pawlowski, A. Kociubiński, M. Duk, in: *SENSORDEVICES 2013, The Fourth Int. Conf. on Sensor Device Technologies and Applications*, 2013, p. 19.